

Experimental and Theoretical Study on Shear Flow Behavior of Polypropylene/Layered Silicate Nanocomposites

Seung Hwan Lee and Jae Ryoun Youn*

Department of Materials Science and Engineering, Seoul National University, 56-1, Shinlim-Dong, Gwanak-Gu, Seoul 151-744, Korea

Received 9 October 2007; accepted 3 December 2007

Abstract

Polypropylene/layered silicate nanocomposites containing maleic anhydride grafted polypropylene were prepared by melt compounding and their rheological behavior was investigated in shear flow. Transient and steady shear flows were simulated numerically by using the K-BKZ integral constitutive equation along with experimentally determined damping functions under dynamic oscillatory and step strain shear flows. Nonlinear shear responses were predicted with the K-BKZ constitutive equation using two different damping functions such as the Wagner and PSM models. It was observed that PP-g-MAH compatibilized PP/layered silicate nanocomposites have stronger and earlier shear thinning and higher steady shear viscosity than pure PP resin or uncompatibilized nanocomposites at low shear rate regions. Strong damping behavior of the PP/layered silicate nanocomposite was predicted under large step shear strain and considered as a result of the strain-induced orientation of the organoclay in the shear flow. Steady shear viscosity of the pure PP and uncompatibilized nanocomposite predicted by the K-BKZ model was in good agreement with the experimental results at all shear rate regions. However, the model was inadequate to predict the steady shear viscosity of PP-g-MAH compatibilized nanocomposites quantitatively because the K-BKZ model overestimates strain-softening damping behavior for PP/layered silicate nanocomposites.

© Koninklijke Brill NV, Leiden, 2008

Keywords

Nanocomposites, rheology, K-BKZ model, damping function, shear flow

1. Introduction

Organic–inorganic nanocomposites are of keen interest since they exhibit excellent properties that may be derived synergistically from the two components. One of the most promising nanocomposites would be hybrids based on an organic polymer and inorganic clay minerals consisting of layered silicates. Polymer/layered silicate nanocomposites become attractive because of their excellent thermal and mechanical properties. They usually show outstanding improvement in tensile modulus,

* To whom correspondence should be addressed. E-mail: jaeryoun@snu.ac.kr

Edited by KSCM

strength, heat distortion temperature, gas and liquid permeability, biodegradability, ionic conductivity and so on [1–3]. But these improved properties are realized only when organoclay particles are well dispersed in the polymer matrix and close inter-particle interactions and hydrodynamic interactions exist. The homogeneous and exfoliated dispersion of the silicate layers, however, could be achieved only in a few cases, e.g. in the presence of polymers containing polar functional groups. This is mostly due to the fact that the silicate layers of the clay have polar hydroxy groups and are compatible with polymers containing polar functional groups. Since polypropylene (PP) does not have any polar groups in its backbone, the homogeneous dispersion of the silicate layers in the polypropylene matrix would not be realized. According to the previous reports [4, 5], however, it was shown that exfoliated PP/layered silicate nanocomposites were obtained when a compatibilizer was added to the combination of PP matrix and organoclay.

Rheology is an important tool for characterization of internal microstructure as well as for understanding polymer processing. Addition of reinforcing fillers into the polymer matrix has become common technology to achieve the required properties, but it also increases its complexity in rheological behavior. Rheological properties of polymer composites are influenced by filler type, size, concentration and surface properties. For example, fillers with plate-like shapes and smaller sizes increase viscosity of polymer melts more than those with the sphere-like shapes and larger sizes. Organoclay has the layered structure of stacked plates of about 1 nm in thickness and 200–1000 nm in planar dimension. Polymer/layered silicate nanocomposites show complex rheological behavior and structural effects such as aggregation or flow-induced orientation of the layered silicates in the polymer matrix [6]. Understanding of the flow behavior is essential to optimize processability of polymer nanocomposites. Therefore, study of the relationship between the viscoelastic behavior of polymer nanocomposite melts and their internal structure is very important from the point of view of industrial applications. Nonlinear rheology deals with flows in which the strain rates and accumulated strains are large or their deformation is fast. Nonlinear viscoelastic behavior of polymer melts often shows extraordinary flow behavior and can be very sensitive to molecular structure.

The nonlinear rheological behaviour of many polymer melts has been reported to be influenced strongly by blending, branching, or compounding of various fillers into the polymer matrix [7, 8]. Since many industrial processes involve large strains and fast strain rates, nonlinear rheology is useful. For example, polymer melts often yield reduced relaxation modulus, strain hardening in extensional flow and thinning in shear flow. These phenomena need nonlinear rheology for modelling and understanding of complicated flows in different geometries. Numerical simulations have been widely used in the field of polymer processing. Constitutive equations are utilized for numerical analysis on the flow and processing of polymer melts or solutions. A proper constitutive equation should be selected for accurate prediction of nonlinear rheological properties such as relaxation modulus, normal stress difference, shear thinning, elongational strain hardening, or corner vortex in the

contraction flow. In general, the choice of constitutive equation depends on the various parameters, e.g. material types, flow patterns and particular applications. The computing technique and accuracy may also play an important role in selecting the constitutive equation.

There have been many studies on rheological properties and theoretical analysis of polymer nanocomposites and many research activities are still ongoing. Rheology and dynamics of polymer nanocomposites filled with nano-sized particles are considerably different from those of conventional composites reinforced with micron-scaled particles. Sarvestani and Picu [9] reported that rheological properties of unentangled composite melts filled with well dispersed nanoparticles were analyzed by using a theoretical network model, which considered strong polymer–filler interactions and molecular chain entanglements. The network kinetics depended on the attachment and detachment dynamics of grafted molecular chains and was modelled by using a set of convection equations for the probability distribution function. A solid-like plateau behavior was predicted well for nanocomposite systems that were formed with network of bonded segments or junctions due to the strong interaction between molecular chains and the nanoparticles. The same authors also analyzed the dynamics and the viscoelasticity of polymer melts and concentrated solutions filled with rigid and spherical nanoparticles numerically by using a frictional molecular model [10]. The dynamics of polymer–filler and filler–filler interactions was considered sufficiently by introducing polymer chain mobility parameter in the model. Polymer chain mobility was reduced in both transverse and longitudinal tube directions because short range energetic interaction between polymer chains and fillers was increased. Toshchevnikov *et al.* [11] studied theoretically the relaxation behavior and viscoelasticity of polymer networks with different friction parameters of monomer and junction sites. They used regular cubic networks topologically built from bead and spring. Dynamic oscillatory shear properties of polymer nanocomposites were analyzed by considering the mean-square displacements of the network segments. Sarvestani *et al.* [12] investigated the rheological properties of the nanocomposites prepared with poly(L-lactide-co-ethylene-oxide-fumarate) and hydroxyapatite nanoparticles and compared the non-Newtonian viscoelastic properties with a linear elastic dumbbell model. A linear elastic dumbbell model was proposed to predict the rheological properties of the polymer nanocomposites at the macroscopic scale. However, it was demonstrated that the nonlinear viscoelastic behavior was controlled by the amplitude of deformation as well as the deformation rate rather than the kinetic rate of the adsorption or desorption of the polymer chains at the surface of nanoparticles.

Although the molecular dynamic (MD) simulation is frequently studied to analyze rheological properties and processing methods of polymer nanocomposites, recent development in numerical simulation techniques makes it possible to apply integral-type constitutive equations to composite melt flow and problems of polymer processing [13, 14]. The K-BKZ constitutive equation has been used to analyze flows of polymeric systems and to perform computer modeling of polymer process-

ing because the model can be used to calculate material functions simply from some rheological measurements. Since the K-BKZ model is based on the general linear viscoelastic model constructed specifically for flows with small displacement gradients, a set of finite strain tensors are used to formulate integral constitutive equation and to describe various flow patterns with large displacement gradients. In addition, the K-BKZ model is now well established for the prediction of rheological properties and to compare the prediction with experimental characterization of polymer melts and solutions. Since this model was applied successfully through the accurate determination of the viscoelastic parameters, e.g. relaxation time spectrum and damping function in a constitutive equation, the model agrees with the experimental results from a phenomenological standpoint. Madiedo *et al.* [15] used a factorable nonlinear viscoelastic model derived from the K-BKZ constitutive equation and modelled nonlinear rheological properties of lubricating grease at very low shear rate. The time dependent part was described by its linear relaxation modulus and a damping function calculated from measured nonlinear relaxation modulus was used as the strain dependent parameter. The K-BKZ model with the Soskey-Winter damping function predicted the transient and steady flows of the lubricating grease well. Wang and Kokini [16] also reported simulation results on nonlinear rheological properties of gluten dough using the K-BKZ constitutive equation with the Wagner damping function. Maia [17] compared two types of models, namely, differential type (Phan-Thien-Tanner model) and integral-type (Wagner model) constitutive equations in describing the behavior of a fluid S1 in simple and complex flows and applied them to theoretical analysis in order to predict the entry pressure drop in axisymmetric flows with contraction ratios in excess of 20:1.

However, very little work has been done on nonlinear rheological properties of polymer/layered silicate nanocomposites by using the integral-type K-BKZ constitutive equation. Ren and Krishnamoorti [18] characterized the dynamic and steady shear flow properties of intercalated nanocomposites of an organically modified layered silicate and a disordered styrene–isoprene diblock copolymer. The K-BKZ constitutive equation was used to predict the steady shear flow properties from the experimentally measured linear relaxation modulus and PSM damping function. While being able to analyze the shear properties at low shear rate ranges, the model failed to predict the steady shear behavior at intermediate shear rates and the normal stress behavior at all shear rates because the nonlinear damping function was inapplicable to the prediction due to overestimated strain-softening behavior of the nanocomposites at intermediate shear rate ranges. However, there have been few studies on qualitative or quantitative evaluation of damping function or numerical analysis on rheological behavior of polymer/layered silicate nanocomposites. In this study, we examined the experimental non-Newtonian rheological behavior of the exfoliated PP/layered silicate nanocomposites and predict the shear flow properties using the K-BKZ integral constitutive equation. In addition, we predicted non-Newtonian rheological behavior of nanocomposites from the K-BKZ model with two different damping functions. Model prediction of the transient and steady

shear viscosities will elucidate the influence of the internal structure on the rheological behavior of the PP/layered silicate nanocomposites.

2. Theoretical Background

Tanner [19] and Bernstein *et al.* [20] proposed an integral-type constitutive model which had been inspired by the theory of rubber-like elasticity. When specialized for the incompressible case, the constitutive model is expressed by equation (1):

$$\sigma(t) = \int_{-\infty}^t m(t-t')h(I_1, I_2)C_t^{-1}(t, t') dt, \quad (1)$$

where $\sigma(t)$ is stress tensor, $m(t-t')$ is the memory function which describes the time dependence of the material and $(t-t')$ is the elapsed time between the remembered past and the present. The memory function is related to the linear relaxation modulus, $G(t)$ and expressed as a sum of exponentials:

$$m(t-t') = \sum_{i=1}^N \frac{G_i}{\lambda_i} \exp\left(-\frac{t-t'}{\lambda_i}\right), \quad (2)$$

where the set of G_i and λ_i defines the relaxation spectra of the material. The Finger strain tensor, $C_t^{-1}(t, t')$, describes the strain imparted to the material and the damping function; $h(I_1, I_2)$, is written as a function of the first and second invariants of the Finger strain tensor.

It is necessary to determine the discrete relaxation modulus from dynamic oscillatory shear measurements, which is done by fitting the experimental data to the generalized Maxwell model. The storage modulus (G'), loss modulus (G''), and linear relaxation modulus are related to the linear relaxation spectrum, $H(\tau)$, by means of the generalized Maxwell equations.

$$G'(\omega) = \sum_{i=1}^N G_i \frac{\omega^2 \lambda_i^2}{1 + \omega^2 \lambda_i^2}, \quad G''(\omega) = \sum_{i=1}^N G_i \frac{\omega \lambda_i}{1 + \omega^2 \lambda_i^2}, \quad (3)$$

$$G(t) = \sum_{i=1}^N G_i \exp\left(-\frac{t}{\lambda_i}\right). \quad (4)$$

In general, linear responses cannot be used to predict the values of material functions for the nonlinear viscoelastic range. To predict the material function, it is necessary to use a nonlinear constitutive equation, such as damping functions. The K-BKZ model is very useful because using a proper damping function enables correct description of various shear and elongational flows. In order to evaluate the damping function, stress relaxation after a sudden step strain is performed in the nonlinear viscoelastic region. Accurate determination of the relaxation modulus is important for fitting of the parameters of various nonlinear damping functions. In

this study, two types of damping functions were examined for the K-BKZ constitutive equation and the optimal parameters for each damping function were estimated. By using these optimal parameters and discrete relaxation spectra, shear viscosity can be predicted. Shear damping function, $h(\gamma)$, can be obtained graphically by evaluating the amount of vertical shift required to superpose the relaxation curve for each nonlinear strain onto the linear curve on a log–log plot. Precisely, it can be obtained as a function of strain, γ , by the vertical shift of the nonlinear relaxation modulus, $G(t, \gamma)$, onto the linear relaxation modulus, $G(t)$

$$h(\gamma) = \frac{G(t, \gamma)}{G(t)}. \quad (5)$$

In the limit of linear viscoelasticity, the linear relaxation modulus is independent of the imposed shear strain. The damping function is unity when the shear strain is small, that is, within the linear viscoelasticity range. As the shear strain increases, the damping function decreases, which can be thought of as the nonlinearity of the relaxation modulus. In general, as the strain becomes large the damping function falls below unity by almost two orders of magnitude [21]. It is worth mentioning that the strain function is not temperature dependent. The temperature affects only the memory function or relaxation modulus through shortening of the relaxation time with increasing temperature [22].

There are two representative forms for the shear damping function in the K-BKZ constitutive equation. One is proposed by Wagner (Wagner model) [23] as follows.

$$h(I) = \exp(-n\sqrt{I-3}), \quad (6)$$

where I is a generalized invariant that is a weighted average of I_1 and I_2 , and n is a parameter that controls the response of the damping function in shear flow. The Wagner model decays very rapidly because of the exponential form, even at low deformation, and therefore it cannot take into account the linear viscoelastic domain. The other is proposed by Papanastasiou *et al.* (PSM model) [24].

$$h(I_1, I_2) = \frac{\alpha}{(\alpha - 3) + \beta I_1 + (1 - \beta)I_2}, \quad (7)$$

where α and β are nonlinear model constants to be determined from shear and elongational flows. In the case of simple shear flow, equation (7) is reduced to the following equation.

$$h(I) = \frac{1}{1 + a(I - 3)}, \quad (8)$$

where a is an adjustable parameter that depends on molecular characteristics and the type of flow. It provides a finite linear viscoelastic region, a steady viscosity in uniaxial elongation, and a well-defined power-law shear viscosity at high shear rate [25].

In this study, we have chosen two types of the damping functions and fit equations (6) and (8) to the experimental data. The K-BKZ integral constitutive equation

for any state of strain may be rewritten as below for the Wagner model (equation (9)) and for the PSM model (equation (10)).

$$\sigma_{12} = \int_{-\infty}^t \sum_{i=1}^N \frac{G_i}{\lambda_i} \exp\left(-\frac{t-t'}{\lambda_i}\right) [\exp(-n\gamma)] \gamma dt', \quad (9)$$

$$\sigma_{12} = \int_{-\infty}^t \sum_{i=1}^N \frac{G_i}{\lambda_i} \exp\left(-\frac{t-t'}{\lambda_i}\right) \left(\frac{\gamma}{1+a\gamma^2}\right) dt'. \quad (10)$$

The transient viscosity growth curves under shear flow are calculated by Wagner model (equation (11)) and PSM model (equation (12)) as follows.

$$\eta^+(t, \dot{\gamma})(t) = \frac{\sigma_{12}(t, \dot{\gamma})}{\dot{\gamma}} = \sum_{i=1}^N \frac{G_i \lambda_i}{(1+n\dot{\gamma}\lambda_i)^2} [1 - \exp(-t)(1 - n\dot{\gamma}\lambda_i t)], \quad (11)$$

$$\begin{aligned} \eta^+(t, \dot{\gamma})(t) &= tG(t) \left(\frac{1}{1+a(\dot{\gamma}t)^2} \right) \\ &+ \int_0^t (t-t') \sum_{i=1}^N \frac{G_i}{\lambda_i} \exp\left(\frac{t-t'}{\lambda_i}\right) \left(\frac{1}{1+a(\dot{\gamma}t)^2} \right) dt'. \quad (12) \end{aligned}$$

3. Experimental

3.1. Materials

Nanocomposites were prepared by compounding isotactic polypropylene (iPP), organophilic layered silicates with a compatibilizer (PP-g-MAH). An isotactic polypropylene homopolymer for sheet extrusion (MOPLENE HP550K, MFR 3.5 g/10 min, Polymirae Co., Korea) was used as the base polymer resin in this study. PP-g-MAH was supplied by Crompton (Polybond[®]3150, USA) and used as a compatibilizer to promote the interaction between the polypropylene matrix and organoclay layers through hydrogen bonding. Its melt flow index was 50 g/10 min and maleic anhydride (g-MAH) content was 0.5 wt%. The layered silicate organoclay was used as the filler for nanocomposite materials. Na⁺-based montmorillonite with the cation-exchange capacity (CEC) of 125 mmol/100 g was supplied by Southern Clay Products (Cloisite[®]15A, USA). The interlayer distance of the organoclay was about 3.45 nm as measured by small-angle X-ray scattering (SAXS).

3.2. Preparation of Nanocomposites

All the samples were prepared by melt compounding with a counter-rotating twin-screw extruder (Brabender PLASTI-CORDER[®]PLE-651). Melt compounding was done at 190°C and at the screw speed of 100 rpm. Prior to extrusion, all the organoclay and compatibilizer were dried in a vacuum oven at 80°C for 8 h. For compar-

Table 1.

Compositions of the prepared nanocomposites based on PP matrix, PP-*g*-MAH compatibilizer and organoclay (wt%)

Sample	Pure PP (MOPLEN HP550K)	PP- <i>g</i> -MAH (Polybond [®] 3150)	Organoclay (Cloisite [®] 15A)
iPP ^a	100	0	0
iPP/00/OLS05 ^b	95	0	5
iPP/05/OLS05 ^c	90	5	5

^a iPP: pure isotactic polypropylene matrix.

^b iPP/00/OLS05: uncompatibilized nanocomposite.

^c iPP/05/OLS05: PP-*g*-MAH compatibilized nanocomposite.

ison, polypropylene nanocomposites with 5.0 wt% organoclay were prepared in the absence or presence of the compatibilizer. The extruded melt was quenched in water and pelletized. For rotational rheological measurements, the pellets were compression moulded into a disk of 25 mm diameter and 1.5 mm thickness. Compositions of the samples are listed in Table 1.

3.3. Characterization

Rheological properties of the polypropylene/layered silicate nanocomposites were investigated with various experimental methods and simulated for transient and steady shear flows using the K-BKZ integral constitutive equation. Two sets of experimental data are needed to find the parameters appearing in the memory function (equation (2)) and shear damping function (equations (6) and (8)), i.e. dynamic oscillatory shear and step strain shear flow data are required. Dynamic oscillatory shear flow measurements were conducted using a rotational rheometer (AR-2000, Rheometric Scientific) with parallel plates. Frequencies of 0.01–200 rad/s were used at the strain amplitude of 10% in order to be within the linear viscoelastic region. Stress relaxation measurements were performed using a controlled strain rheometer (ARES, Rheometric Scientific) with a parallel plate shear flow device with the maximum strain of 500%. In these experiments, parallel plates with the diameter of 25 mm and the gap size of 1.0 mm were used.

To compare simulation results with experimental data for steady shear flow, steady flow measurements were carried out using two types of rheometer. Rotational (AR-2000, Rheometric Scientific) and capillary (Rheograph-2003, Göttfert) rheometers were used at low and high shear rates, respectively. Parallel plate geometry was used to measure the steady shear viscosity with respect to shear rates of 0.001 to 10 s⁻¹. In the parallel plate instrument, two plates with the diameter of 25 mm and the gap size of 1.0 mm were also used. A capillary rheometer was used to measure the steady shear viscosity with respect to shear rate of 10 to 1000 s⁻¹. A capillary with the diameter of 1.0 mm and the length/diameter ratio of 30 was used and measurements were carried out at 190°C.

4. Results and Discussion

4.1. Linear Viscoelastic Behavior

Dynamic oscillatory shear flow was employed to evaluate linear viscoelastic properties of polypropylene/layered silicate nanocomposites and to obtain relaxation parameters of the memory function. The memory function is independent of the strain-dependent damping function and the parameters can be determined from dynamic oscillatory shear measurement. The storage and loss moduli were measured for pure PP matrix, uncompatibilized nanocomposites and PP-g-MAH compatibilized nanocomposites at 190°C. Figure 1 shows variation of the dynamic oscillatory shear properties of the three samples within the linear viscoelastic range. Storage modulus, loss modulus and complex viscosity are plotted as a function of angular frequency at steady state. The pure polypropylene shows classical viscoelastic behavior, i.e. a terminal flow region at low frequencies where storage and loss moduli are proportional to ω^2 and ω , respectively. The uncompatibilized nanocomposite shows small deviations from the classical behavior in the case of storage and loss moduli at low frequencies. However, dynamic oscillatory properties of the PP-g-MAH compatibilized nanocomposites are distinctly different from those of pure polypropylene and uncompatibilized nanocomposites. While the pure polypropylene shows Newtonian plateau behavior at low frequency region, stronger and earlier shear thinning behavior is observed in the

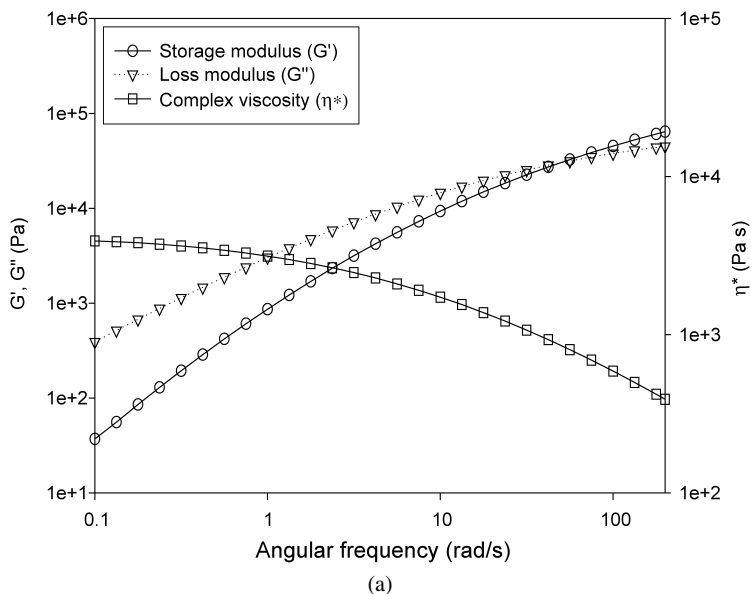
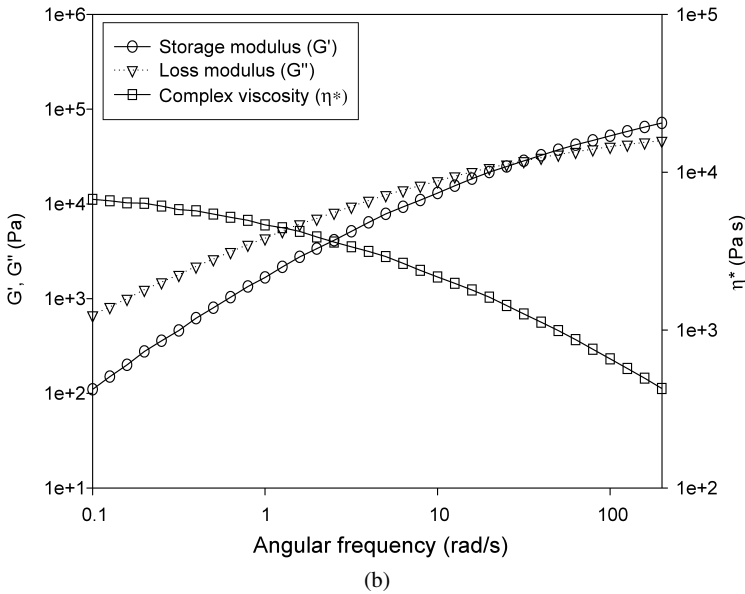
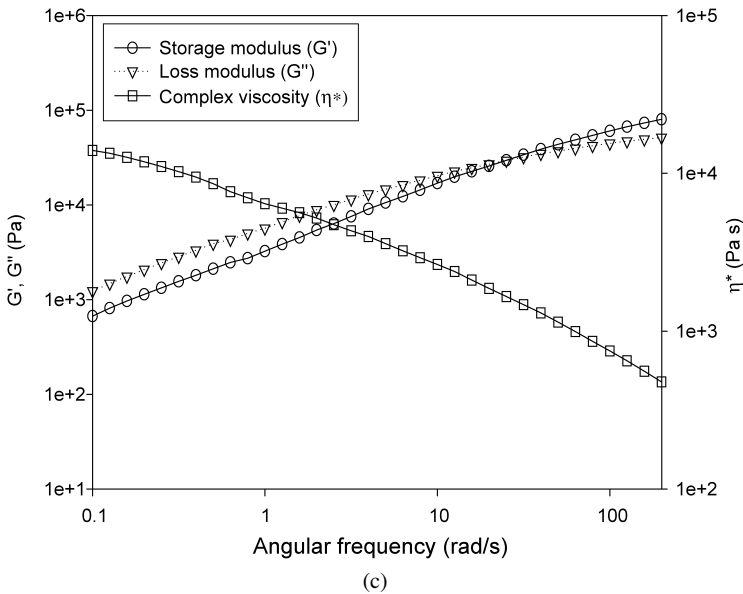


Figure 1. Variation of the dynamic oscillatory shear properties of (a) pure PP (iPP), (b) uncompatibilized nanocomposite (iPP/00/OLS05) and (c) PP-g-MAH compatibilized nanocomposite (iPP/05/OLS05) with respect to angular frequency (ω) and full line indicating a fit obtained from the linear relaxation spectrum of Table 2.



(b)



(c)

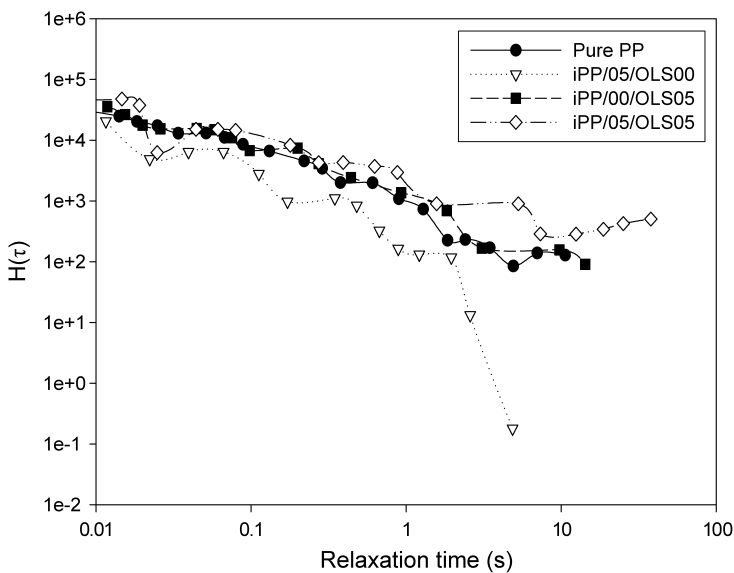
Figure 1. (Continued.)

case of the compatibilized nanocomposite. At low frequency region, storage modulus shows non-terminal solid-like plateau behavior and has higher value than that of pure PP or uncompatibilized nanocomposites. As the amount of well-dispersed organoclay is increased by adding the compatibilizer, a network structure will be formed due to the close interaction between clay particles as well as strong interaction between organoclay particles and PP molecular chains [26]. At

Table 2.

Discrete relaxation spectra calculated from generalized Maxwell model

iPP		iPP/00/OLS05		iPP/05/OLS05	
λ_i (s)	G_i (Pa)	λ_i (s)	G_i (Pa)	λ_i (s)	G_i (Pa)
0.00574	78 620	0.00575	83 240	0.005925	92 990
0.03683	18 790	0.04465	23 350	0.05312	28 790
0.1248	9792	0.1551	6113	0.3420	8631
0.6320	2813	0.4356	3058	1.167	578.2
4.662	277.7	1.567	1082	1.539	736.5
				8.648	1349

**Figure 2.** Discrete relaxation spectrum, $H(\tau)$, calculated from generalized Maxwell model using TA Analysis software (iPP/05/OLS00: PP-Polybond[®] 3150 blend).

high frequency, the storage modulus of the PP-g-MAH compatibilized nanocomposite is similar to that of pure polypropylene matrix, indicating that segmental motion of the polymer matrix determines the material response at short time scales.

Calculation of the relaxation spectrum from the linear viscoelastic function is necessary to estimate other linear viscoelasticity functions. In general, it has been calculated from the storage and loss moduli by a nonlinear minimization procedure [27]. In this study, a discrete relaxation spectrum was obtained by fitting the linear viscoelastic function to a generalized Maxwell model and their shapes were compared for the pure PP, uncompatibilized nanocomposites and PP-g-MAH compatibilized nanocomposites. It was observed in Fig. 2 that the PP-g-MAH

compatibilized nanocomposite produces a large shift of the spectra toward longer relaxation time scales. Complete polymer relaxation is retarded by the two-phase structure created by the layered silicate organoclay dispersed in the polypropylene matrix as well as by the strong molecular interaction between polypropylene matrix and layered silicate organoclay [28]. Table 2 shows a set of relaxation parameters determined from dynamic oscillatory shear measurements. The relaxation values listed in Table 2 enable a good curve fitting of the experimentally obtained storage and loss moduli as shown in Fig. 1. It was shown that the relaxation spectra are shifted considerably by addition of organoclay and compatibilizer such that the samples have longer relaxation time in the order of PP-g-MAH compatibilized nanocomposites, uncompatibilized composites and pure polypropylene matrix. Krishnamoorti and colleagues [29] proposed that the presence of silicate layers alone is not sufficient to produce the non-terminal solid-like flow behavior of exfoliated nanocomposites. The internal structure of silicate layers oriented in preferable direction and incomplete relaxation of the polymer chains contribute to the solid-like behavior of polymer nanocomposites at low frequencies. In this study, it is shown that two-phase structure of the compatibilized polypropylene/layered silicate nanocomposite causes retardation of the complete polymer chain relaxation.

4.2. Stress Relaxation and Damping Function

Effects of strain amplitude on the stress relaxation behavior were examined by using step strain measurement. Figure 3 shows evolution of the relaxation modulus

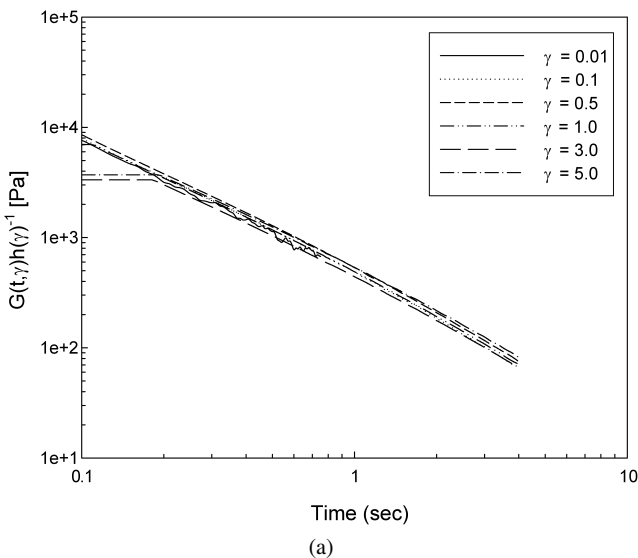


Figure 3. Evolution of the linear and nonlinear relaxation moduli of (a) pure PP, (b) uncompatibilized nanocomposite and (c) PP-g-MAH compatibilized nanocomposite with respect to the elapsed time after step shear strain at 190°C.

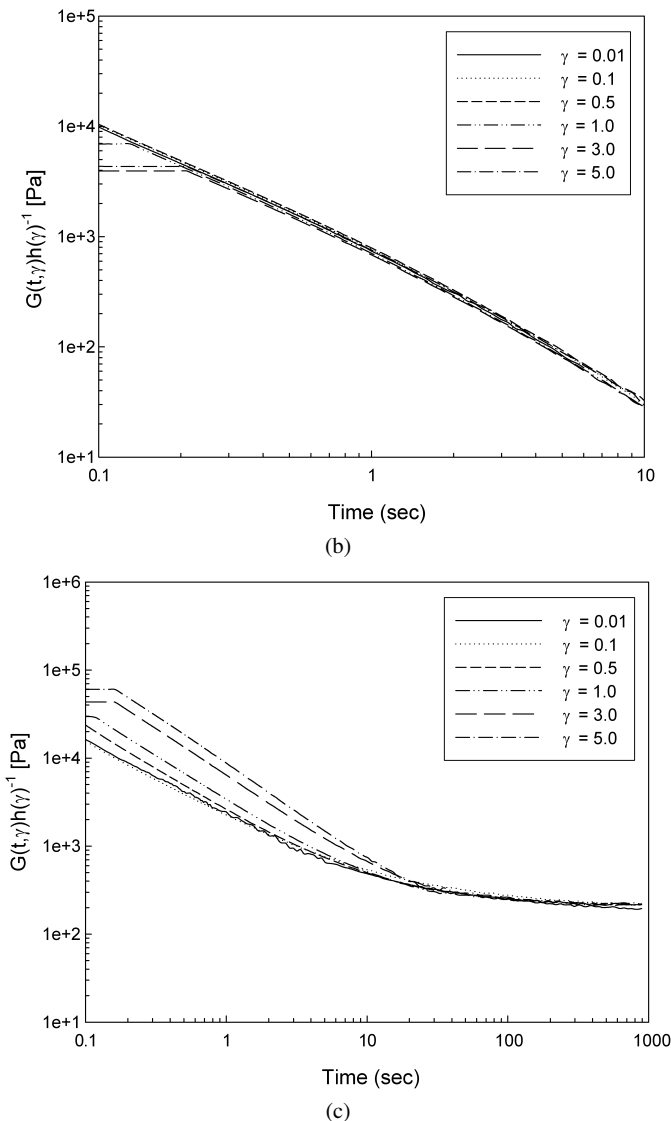


Figure 3. (Continued.)

with respect to the elapsed time after a sudden step shear strain where the amplitude of the strain was varied from linear to nonlinear viscoelasticity ranges. Plotting of $G(t, \gamma)/h(\gamma)$ versus time (t) is displayed for the three samples at strains of 1, 10, 50, 100, 300 and 500%. It is evident from the data shown in the figure that time–strain separability is valid for the range of applied strains. However, it is noteworthy that time–strain separability is approximate, i.e. $G(t, \gamma)/h(\gamma)$ data obtained at multiple shear strains do not collapse to a single line [30]. The data of $G(t, \gamma)/h(\gamma)$ were independent of time for pure polypropylene and un-

compatibilized nanocomposites. In this case, time–strain separability has been investigated to predict the nonlinear rheological responses of many polymer materials. Relaxation modulus was still kept in shape when the shear strain amplitude was increased and the relaxation modulus was separated into time and strain dependent functions. In contrast, PP-*g*-MAH compatibilized nanocomposites show slower stress relaxation behavior than pure polypropylene and uncompatibilized nanocomposites, as shown in Fig. 3(c). Although time–strain separability is observed in about 30 s, plots of $G(t, \gamma)/h(\gamma)$ reveal rather unusual and complex time dependence over a broad time range. The step shear strain alters nonlinear viscoelastic response of the compatibilized nanocomposite more strongly than that of the pure polypropylene or uncompatibilized nanocomposite because microstructure of the compatibilized nanocomposite is more strain-dependent. As may be deduced, earlier and stronger structural destruction will take place due to strong shear flow in compatibilized polypropylene/layered silicate nanocomposites. The reason why structural destruction occurred is that three dimensional network formed among the layered silicate organoclay and the PP molecular chain, and the compatibilizer is more sensitive to shear flow than that of the uncompatibilized nanocomposite. Therefore, network structure may be destroyed and aligned earlier than with pure PP matrix or uncompatibilized composites as shown in damping functions for the three types of materials (Fig. 4).

The damping function has been adjusted in order to insure the best prediction of the K-BKZ constitutive equation in shear flow. In Fig. 4, strain dependence of the damping function is adequately fitted by the relationship that has been frequently used to predict the damping behavior in complex polymer systems [20, 31]. It shows a comparison between the Wagner and PSM damping functions obtained from the step strain shear measurement. The damping function for the PP-*g*-MAH compatibilized nanocomposite differs from those of pure polypropylene and uncompatibilized nanocomposites. Although pure polypropylene and uncompatibilized nanocomposites exhibit similar damping behavior, i.e. delayed damping behavior, the compatibilized nanocomposites show strong strain-softening behavior with low onset strain amplitude. The strain-softening behavior is related to the strain-induced alignment of the multilayered organoclay domains in the shearing direction because the alignment plays an important role in damping of compatibilized nanocomposites. The increase in the amount of organoclay or compatibilizer may increase the sensitivity of the microstructure to alignment and orientation under shear flow [32]. The mathematical forms of the Wagner and PSM models under shear flow are chosen to fit the experimental data obtained from step strain shear flow. The first and second strain invariants are identical with each other under shear deformation. The damping function, $h(I_1, I_2)$, in shear flow is the same as the shear damping function, $h(\gamma)$. Figure 4 shows the shear damping function as a function of shear strain, γ . The parameter values used in the fitting procedure are presented in Table 3. The Wagner and PSM damping functions

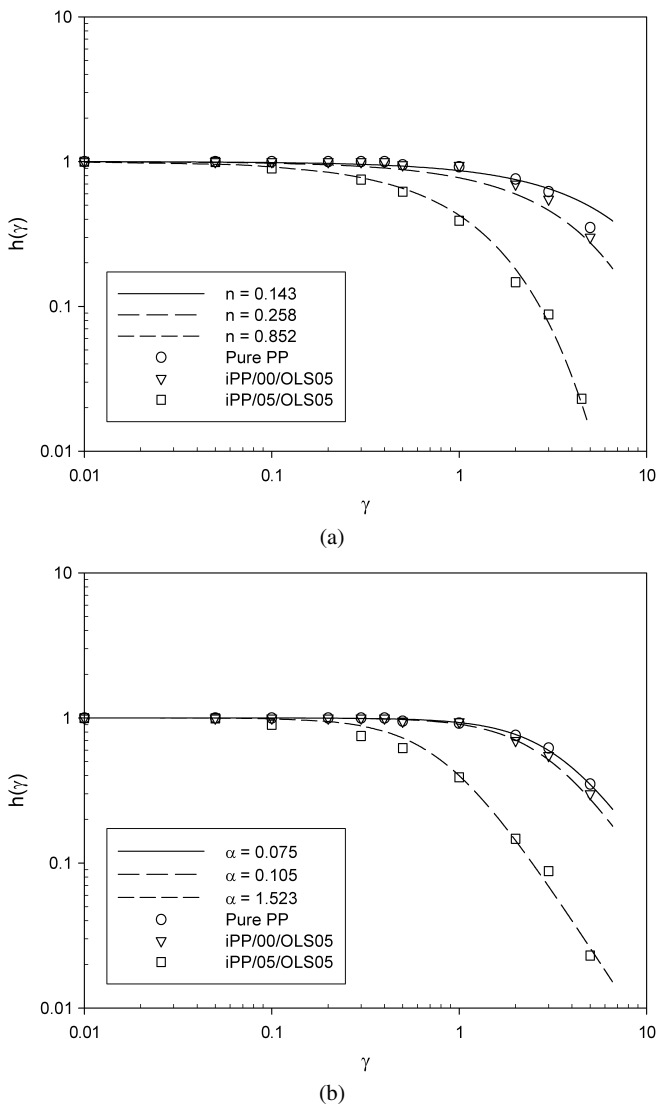


Figure 4. (a) Wagner and (b) PSM shear damping functions (lines) for pure PP (○), uncompatibilized nanocomposite (▽) and compatibilized nanocomposite (□) obtained from step shear experiments at 190°C.

are described for the three samples. In the case of compatibilized nanocomposites, the damping parameter is increased more rapidly than those of pure polypropylene and uncompatibilized nanocomposites. The rapid increase of the damping parameter can be explained by resistance of junctions against increasing strain and by the macromolecular structure with branches which might hinder complete retraction of the molecular chains leading to conservation of network junctions [33, 34].

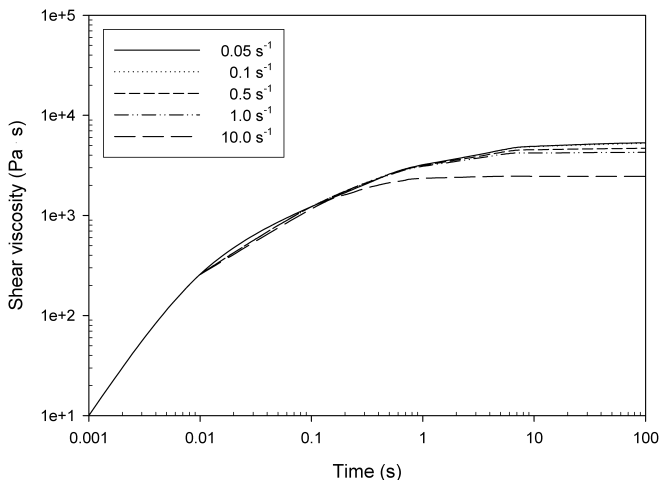
Table 3.
Fitting parameter of each damping model for the three samples

	Fitting parameter
Wagner model	n
iPP	0.143
iPP/00/OLS05	0.258
iPP/05/OLS05	0.852
PSM model	a
iPP	0.075
iPP/00/OLS05	0.105
iPP/05/OLS05	1.523

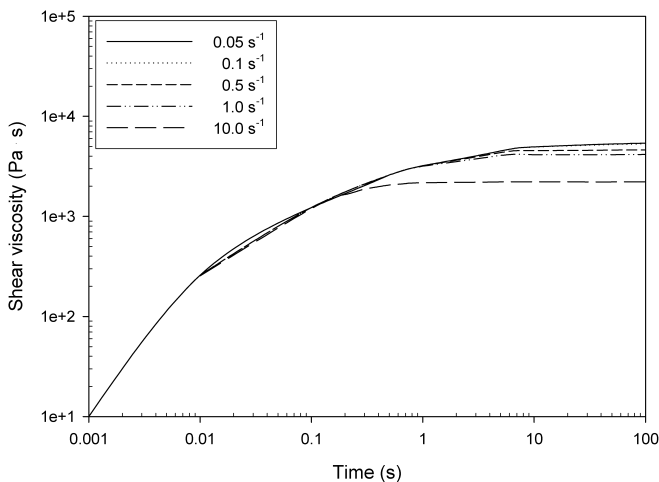
4.3. Transient Shear Flow

The viscosity growth on the inception of steady shear flow, $\eta^+(\dot{\gamma}, t)$, was calculated by applying the memory function and two types of damping functions in the K-BKZ constitutive equation. In Fig. 5, shear viscosity growth curves are shown for pure polypropylene melts at 190°C. The shear viscosity quickly reaches a steady plateau value in about 5 to 10 s after application of the shearing flow and stress overshoot behavior is not predicted at all shear rates. The maximum and steady state values of the transient shear viscosity are obtained at shorter time as the shear rate is increased. In general, the time at which viscosity growth curve departs from the linear envelope is decreased as the shear rate is increased such that the shear strain where nonlinear effects are first detected is constant [35].

Shear viscosity growth curves of the uncompatibilized nanocomposite melts are predicted by the Wagner and PSM models under transient shear flow as shown in Fig. 6. Similar results are obtained for PP matrix as shown in Fig. 5. Since the viscosity decreases with increase in the shear rate, shear viscosity approaches successively lower steady state asymptotes as the shear rate is raised. It is well known that the maximum point in transient shear growth curve always occurs at about the same value of the shear strain, $\gamma_{\max} = t_{\max}\dot{\gamma}$, for a given polymer and that γ_{\max} is on the order of 2 to 3 [36]. Figure 7 shows shear viscosity growth curves of PP-*g*-MAH compatibilized nanocomposite melts. Transient shear viscosity exhibits a slight stress overshoot only at the highest applied shear rate of 10 s⁻¹. At lower shear rates, a stable plateau was reached within about 100 s after application of the shear field. Given that the constitutive equation is a valid representation for the behavior of compatibilized nanocomposite melts, it is clear that the samples show a trend to weaker damping function as molecular branching or networking increases [37]. In this case, transient viscosities approach steady state values more quickly than those of pure PP and uncompatibilized nanocomposite as the shear rate increases.



(a)

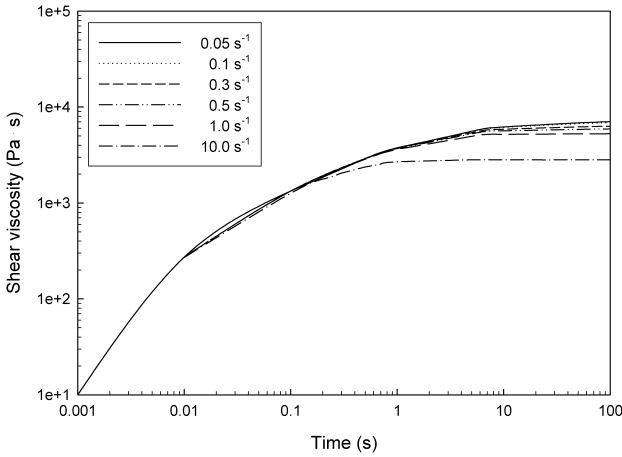


(b)

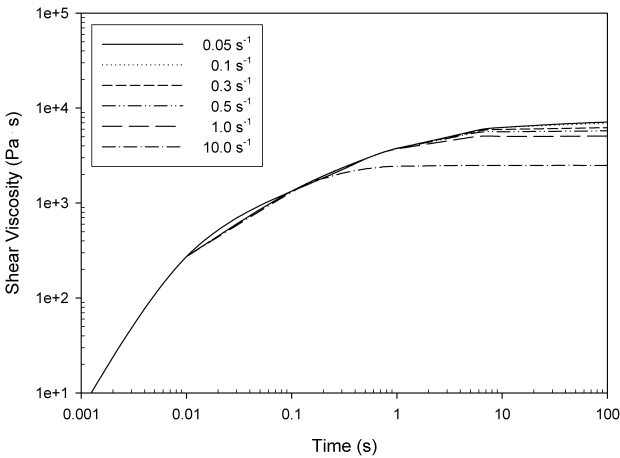
Figure 5. Comparison of the (a) Wagner and (b) PSM model predictions on shear viscosity growth curves, $\eta^+(\dot{\gamma}, t)$, in transient shear flow for pure PP melts.

4.4. Steady Shear Flow

Predicted results of the Wagner and PSM models are compared with experimental data for steady shear viscosity of the pure polypropylene and two different nanocomposites. All the samples exhibit shear thinning behavior over the entire shear rate ranges. In Fig. 8, the Wagner and PSM model predictions are compared with measured shear viscosity in the steady state for pure polypropylene. Results of the steady state measurements show that pure polypropylene matrix tends to have a zero-shear-rate viscosity at the shear rate below 0.3 s^{-1} . Once the characteristic shear rate is exceeded, the steady shear viscosity is a function of the shear rate



(a)

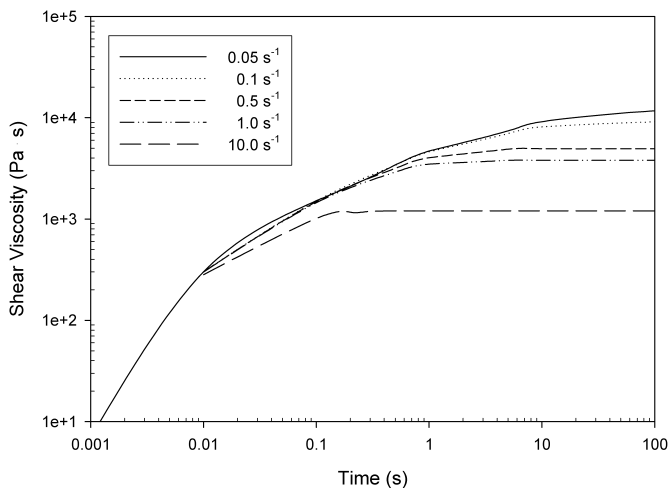


(b)

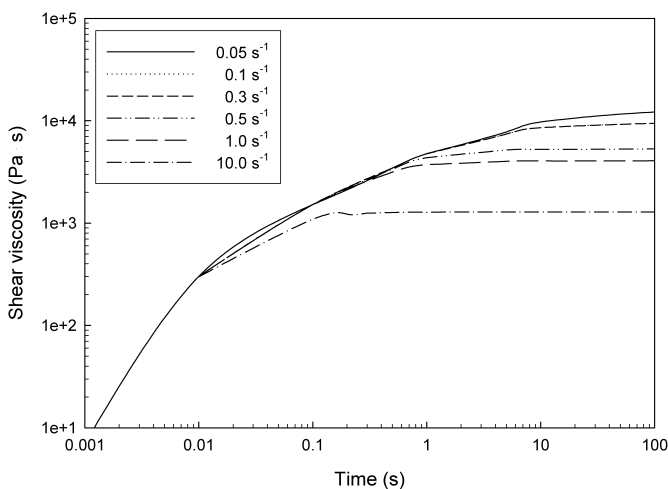
Figure 6. Comparison of the (a) Wagner and (b) PSM model predictions on shear viscosity growth curves, $\eta^+(\dot{\gamma}, t)$, in transient shear flow for uncompatibilized nanocomposite (iPP/00/OLS05) melts.

and follows the power-law. In the experimental range of the shear rate, the Wagner and PSM models demonstrated their capability to predict zero-shear-rate viscosity in the lower shear rate region and power-law dependence in the higher shear rate region, respectively. The model predictions for uncompatibilized nanocomposites are displayed and compared with measured shear viscosity in Fig. 9. The Wagner model predicts the observed zero-shear-rate viscosity at the low shear rate region (below 0.3 s^{-1}) and shear thinning at the higher shear rate region. However, the PSM model underestimates values in comparison with the experimental results in the high shear rate region above 10 s^{-1} .

Figure 10 compares measured viscosity of the PP-g-MAH compatibilized nanocomposite with those predicted by the Wagner and PSM models at steady state.



(a)



(b)

Figure 7. Comparison of the (a) Wagner and (b) PSM model predictions on shear viscosity growth curves, $\eta^+(\dot{\gamma}, t)$, in transient shear flow for PP-g-MAH compatibilized nanocomposite (iPP/05/OLS05) melts.

They show stronger and earlier shear thinning behavior than pure polypropylene and uncompatibilized nanocomposite melts. It is anticipated that the organoclay particles will be aligned in the flow direction under shear force. The Wagner and PSM model predictions seem to show good agreement with experimental data in the shear rate range of $\dot{\gamma} < 1.0$. Model predictions, however, underestimate the viscosity compared with experimental data at intermediate and higher shear rate regions (especially 10 to 1000 s^{-1}) because they have strong damping behavior at large strains. Generally, polymer/layered silicate nanocomposites exhibit signifi-

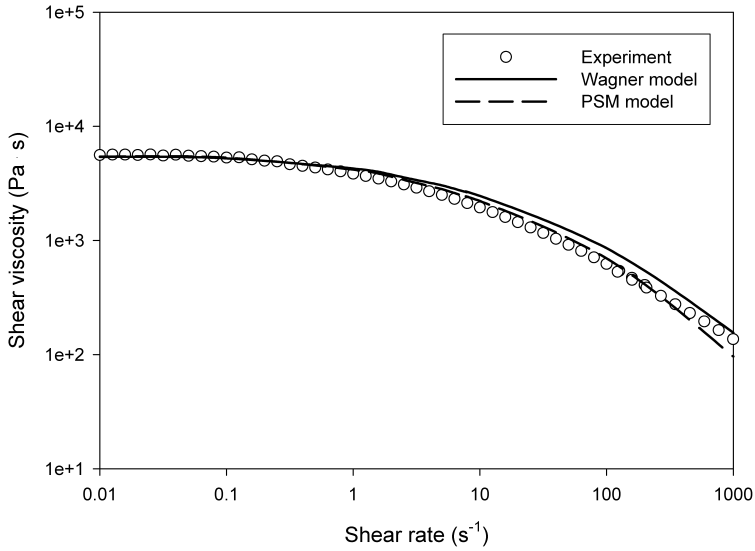


Figure 8. Comparison of Wagner and PSM model predictions with experimental shear viscosity in steady state functions for pure polypropylene (iPP) melts at 190°C.

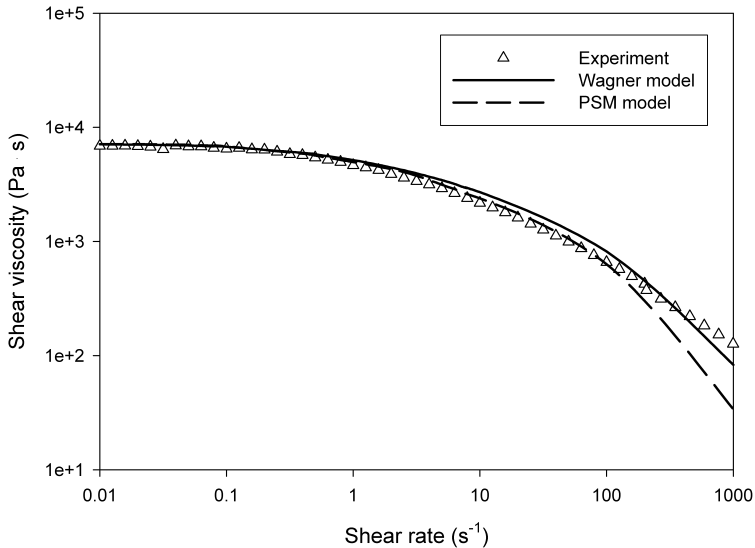


Figure 9. Comparison of Wagner and PSM model predictions with experimental shear viscosity in steady state functions for uncompatibilized nanocomposite melts (iPP/00/OLS05) at 190°C.

cant deviations from the Cox–Merz rule, while all pure polymers obey the empirical relation. According to previous reports [26, 38, 39], two possible reasons were provided for the deviation from the Cox–Merz rule in the case of nanocomposites. First, the Cox–Merz rule is applicable only to homogenous systems like homopoly-

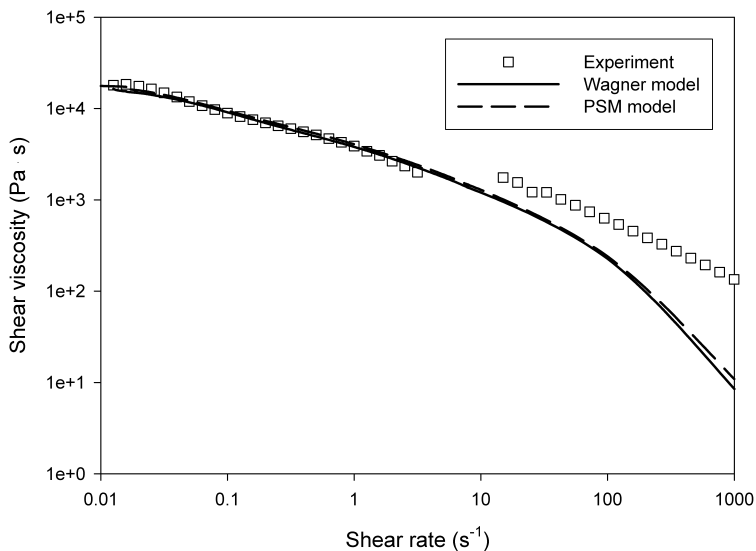


Figure 10. Comparison of Wagner and PSM model predictions with experimental shear viscosity in steady state functions for PP-*g*-MAH compatibilized nanocomposite melts (iPP/05/OLS05) at 190°C.

mer melts, but nanocomposites are heterogeneous systems. Second, formation of the layered organoclay structure is different when nanocomposites are subject to dynamic oscillatory shear and steady shear flows. The resistance to flow for small amplitude oscillatory motion is much larger than that for steady shear flow where shear strain is increasing continuously.

Ren and Krishnamoorti [18] and Valencia *et al.* [40] also reported that the K-BKZ model predicts stronger shear thinning behavior than that observed experimentally and underpredicts the experimental data at intermediate shear rate regions. According to their reports, the K-BKZ model is unable to calculate the viscoelastic properties at high shear rates because the linear stress relaxation modulus needs to be extrapolated to shorter time scales and can be used only to predict the low shear rate dependence. Since the K-BKZ model employs linear stress relaxation modulus data and step strain measurement results to describe the nonlinear damping function, it is clearly inadequate for the model to predict the viscosity of the polymer nanocomposite at all shear rates. During steady shear test the sample evolves slowly to a final mesoscale structure with increase in the extent of orientation which depends on the shear rate. They proposed that the inability of the K-BKZ model in predicting the intermediate shear rate viscosity implies that the nanocomposites undergo changes in their mesoscale structure at the shear rate and exhibit rheological behavior which can not be predicted by the damping functions determined by the step-strain measurement. However, predicted viscosity of the PP-*g*-MAH compatibilized nanocomposite shows slight deviation from the experimental results at low strain rates.

5. Conclusions

PP/layered silicate nanocomposites were prepared by the melt compounding and their rheological behavior was examined in shear flow. The rheological behavior was studied numerically using the K-BKZ integral constitutive equation and investigated experimentally in dynamic oscillatory shear and step strain shear flows. The constitutive equation was evaluated in transient and steady shear flows using Wagner and PSM damping functions and the results were compared with measured steady shear viscosity. A discrete relaxation spectrum was obtained by fitting the linear viscoelasticity function to a generalized Maxwell model. It was confirmed that the spectrum of the compatibilized nanocomposite is shifted toward the longer relaxation time scales due to strong molecular interaction between polypropylene matrix and organoclay in nanocomposites. Stress relaxation measurements were carried out to obtain damping functions in the nonlinear viscoelastic region and optimal parameters for each damping function were estimated. By using these parameters and the discrete relaxation spectrum, transient and steady shear viscosities were calculated and interpreted. The K-BKZ model showed good quantitative prediction of rheological behavior of pure polypropylene and uncompatibilized nanocomposites in steady shear flows. However, it was inadequate to predict shear viscosity behavior of the compatibilized polypropylene/layered silicate nanocomposites. The K-BKZ model prediction showed good agreement with experimental data in the low and intermediate shear rate ranges, but it predicted underestimated values compared with experimental data in the high shear rate region. It was found that the compatibilized nanocomposites have strong damping behavior due to the strain-induced alignment of the layered silicate organoclay in shear flow.

Acknowledgements

This study was financially supported by the Applied Rheology Center (ARC) at Korea University. The authors are grateful for the support.

References

1. S. S. Ray and M. Okamoto, Polymer/layered silicate nanocomposites: a review from preparation to processing, *Prog. Polym. Sci.* **28**, 1539–1641 (2003).
2. D. G. Seong, T. J. Kang and J. R. Youn, Rheological characterization of polymer based nanocomposites with different nanoscale dispersions, *e-Polymers* **005**, 1–14 (2005).
3. S. K. Lee, D. G. Seong and J. R. Youn, Degradation and rheological properties of biodegradable nanocomposites prepared by melt intercalation method, *Fiber. Polym.* **6**, 289–296 (2005).
4. M. Kawasumi, N. Hasegawa, M. Kato, A. Usuki and A. Okada, Preparation and mechanical properties of polypropylene-clay hybrid, *Macromolecules* **30**, 6333–6338 (1997).
5. R. Krishnamoorti and K. Yurekli, Rheology of polymer layered silicate nanocomposites, *Curr. Opin. Coll. Interf. Sci.* **6**, 464–470 (2001).
6. Y. H. Hyun, S. T. Lim, H. J. Choi and M. S. Jhon, Rheology of poly(ethylene oxide)/organoclay nanocomposites, *Macromolecules* **34**, 8084–8093 (2001).

7. A. Lele, M. Mackley, G. Galgali and C. J. Ramesh, *In situ* rheo-x-ray investigation of flow-induced orientation in layered silicate–syndiotactic polypropylene nanocomposite melt, *J. Rheol.* **46**, 1091–1110 (2002).
8. A. D. Gotsis and B. L. F. Zeevenhoven, Effect of long branches on the rheology of polypropylene, *J. Rheol.* **48**, 895–914 (2004).
9. A. S. Sarvestani and C. R. Picu, Network model for the viscoelastic behavior of polymer nanocomposites, *Polymer* **45**, 7779–7790 (2004).
10. A. S. Sarvestani and C. R. Picu, A frictional molecular model for the viscoelasticity of entangled polymer nanocomposites, *Rheol. Acta.* **45**, 132–141 (2005).
11. V. P. Toshchevnikov, A. Blumen and Y. Y. Gotlib, Dynamics of polymer networks with strong differences in the viscose characteristics of their crosslinks and strand, *Macromol. Theory Simul.* **16**, 359–377 (2007).
12. A. S. Sarvestani, X. He and E. Jabbari, Viscoelastic characterization and modeling of gelation kinetics of injectable *in situ* crosslinkable poly(lactide-ethylene oxide-fumarate) hydrogels, *Bio-macromolecules* **8**, 406–412 (2007).
13. A. Nishioka, T. Takahashi, Y. Masubuchi, J. Takimoto and K. Koyama, Description of uniaxial, biaxial, and planar elongational viscosities of polystyrene melt by the K-BKZ model, *J. Non-Newtonian Fluid Mech.* **89**, 287–301 (2000).
14. F. Erchiqui, Thermodynamic approach of inflation process of K-BKZ polymer sheet with respect to thermoforming, *Polym. Engng. Sci.* **45**, 1319–1335 (2005).
15. J. M. Madiedo, J. M. Franco, V. Valencia and C. Gallegos, Modeling of the non-linear rheological behavior of a lubricating grease at low-shear rates, *J. Tribol.* **122**, 590–596 (2000).
16. C. F. Wang and J. L. Kokini, Simulation of the nonlinear rheological properties of gluten using the Wagner constitutive model, *J. Rheol.* **39**, 1465–1482 (1995).
17. J. M. Maia, Theoretical modelling of fluid S1: a comparative study of constitutive models in simple and complex flows, *J. Non-Newtonian Fluid Mech.* **85**, 107–125 (1999).
18. J. Ren and R. Krishnamoorti, Nonlinear viscoelastic properties of layered-silicate-based intercalated nanocomposites, *Macromolecules* **36**, 4443–4451 (2003).
19. R. I. Tanner, From A to (BK)Z in constitutive relations, *J. Rheol.* **32**, 673–702 (1988).
20. B. Bernstein, E. A. Kearsley and L. J. Zapas, A study of stress relaxation with finite strain, *Trans. Soc. Rheol.* **7**, 391–410 (1963).
21. K. Osaki, On the damping function of shear relaxation modulus for entangled polymers, *Rheol. Acta.* **32**, 429–437 (1993).
22. H. M. Laun, Description of the non-linear shear behaviour of a low density polyethylene melt by means of an experimentally determined strain dependent memory function, *Rheol. Acta.* **17**, 1–15 (1978).
23. M. H. Wagner, Analysis of time-dependent non-linear stress-growth data for shear and elongational flow of a low-density branched polyethylene melt, *Rheol. Acta.* **18**, 33–50 (1979).
24. A. C. Papanastasiou, L. E. Scriven and C. W. Macosko, An integral constitutive equation for mixed flows: viscoelastic characterization, *J. Rheol.* **27**, 387–410 (1983).
25. G. Barakos, E. Mitsoulis, C. Tzoganakis and T. Kajiwara, Rheological characterization of controlled-rheology polypropylenes using integral constitutive equations, *J. Appl. Polym. Sci.* **59**, 543–556 (1996).
26. S. H. Lee, E. Cho and J. R. Youn, Rheological behavior of polypropylene/layered silicate nanocomposites prepared by melt compounding in shear and elongational flows, *J. Appl. Polym. Sci.* **103**, 3506–3513 (2007).
27. J. D. Ferry, *Viscoelastic Properties of Polymers*. Wiley, New York, USA (1980).

28. R. Kotsilkova, Rheology-structure relationship of polymer/layered silicate hybrids, *Mech. Time-Depend Mater.* **6**, 283–300 (2006).
29. J. Ren, A. S. Silva and R. Krishnamoorti, Linear viscoelasticity of disordered polystyrene polyisoprene block copolymer bases layered-silicate nanocomposites, *Macromolecules* **33**, 3739–3746 (2000).
30. M. T. Islam, M. T. J. Sanchez-Reyes and L. A. Archer, Nonlinear rheology of highly entangled polymer liquids: step shear damping function, *J. Rheol.* **45**, 61–82 (2001).
31. M. Isaki, M. Takahashi and O. Urakawa, Biaxial damping function of entangled monodisperse polystyrene melts: comparison with the Mead-Larson-Doi model, *J. Rheol.* **47**, 1201–1210 (2003).
32. M. Iza and M. Bousmina, Damping function for narrow and large molecular weight polymers: comparison with the force-balanced network model, *Rheol. Acta.* **44**, 372–378 (2005).
33. M. H. Wagner, S. Kheirandish and O. Hassager, Quantitative prediction of transient and steady-state elongational viscosity of nearly monodisperse polystyrene melts, *J. Rheol.* **49**, 1317–1327 (2005).
34. M. Sugimoto, Y. Masubuchi, J. Takimoto and K. Koyama, Melt rheology of polypropylene containing small amount of high molecular weight chain I. shear flow, *J. Polym. Sci. Pol. Phys.* **39**, 2692–2704 (2001).
35. M. H. Wagner and J. Meissner, Network disentanglement and time-dependent flow behaviour of polymer melts, *Macromol. Chem.* **181**, 1533–1550 (1980).
36. R. G. Larson, *The Structure and Rheology of Complex Fluids*. Oxford University Press, New York, USA (1999).
37. J. Kasehagen and C. W. Macosko, Nonlinear shear and extensional rheology of long-chain randomly branched polybutadiene, *J. Rheol.* **42**, 1303–1327 (1998).
38. R. Devendra, S. Hatzikiriakos and R. Vogel, Rheology of metallocene polyethylene-based nanocomposites: influence of graft modification, *J. Rheol.* **50**, 415–434 (2006).
39. X. He, J. Yang, L. Zhu, B. Wang, G. Sun, P. Lv, I. Y. Phang and T. Liu, Morphology and melt rheology of nylon 11/clay nanocomposites, *J. Appl. Polym. Sci.* **102**, 542–549 (2006).
40. C. Valencia, M. C. Sanchez, A. Ciruelos, A. Latorre, J. M. Madiedo and C. Gallegos, Non-linear viscoelasticity modeling of tomato paste products, *Food Res. Int.* **36**, 911–919 (2003).